

Dramatic enhancement of visible-light absorption in TiO_2 by adding Bi

Fernando P. Sabino

*Department of Materials Science and Engineering,
University of Delaware, Newark, Delaware 19716, USA and*

Centro de Ciências Naturais e Humanas, Universidade Federal do ABC, Santo André, São Paulo, 09210-580, Brazil

Anderson Janotti

*Department of Materials Science and Engineering,
University of Delaware, Newark, Delaware 19716, USA*

TiO_2 is a wide band-gap semiconductor that has been intensively investigated for photocatalysis and water-splitting. However, weak light absorption in the visible region of the spectrum poses stringent limitation to its practical application. Doping of TiO_2 with N or transition-metal impurities has been explored to shift the onset of optical absorption to the visible region, yet with limited success. Based on hybrid density functional calculations, we propose adding Bi to TiO_2 , in the form of dilute $\text{Ti}_{1-x}\text{Bi}_x\text{O}_2$ alloys, to efficiently shift the optical absorption to the visible region. Compared to N, Bi introduces an intermediate valence band that is significantly higher in the band gap, and leaves the conduction band almost unchanged, leading to a remarkable redshift in the absorption coefficient to cover almost all the visible-light spectrum. Comparing formation enthalpies, our results show that adding Bi costs significantly less energy than N in oxidizing conditions, and that $\text{Ti}_{1-x}\text{Bi}_x\text{O}_2$ might make a much more efficient photocatalyst than $\text{TiO}_{2-y}\text{N}_y$ for water splitting.

INTRODUCTION

Solar energy is an abundant, clean, and renewable energy resource, and our ability to efficiently harness and use it is key for an energy sustainable future [1]. Artificial photosynthesis, and photocatalysis in general, is a promising technology to harvest and store solar energy, producing hydrogen or hydrocarbons via water splitting or CO_2 transformation using a photoelectrochemical device [2, 3]. It remains a significant challenge to fabricate an efficient and stable solar-energy conversion device. Controlling the semiconductor properties in these devices is of primary concern in the development of new materials for solar-energy conversion. Among the semiconductor materials that have been explored as photoelectrodes, TiO_2 stands out as being composed of earth-abundant and non toxic elements, and being photochemically stable under acidic and basic conditions [4–7]. However, the large band gap of 3.0 eV for rutile and 3.2 eV for anatase severely limit the performance of TiO_2 since only 5% of the solar spectrum can in principle be utilized [6, 8, 9].

Attempts have been made to extend light absorption in TiO_2 to the visible region by adding impurities (doping) or forming dilute alloys, while maintaining the photochemical stability and low cost. Adding N has been considered one of the most effective way to bring light absorption in TiO_2 to the visible range [7, 10–15]. The $2p$ orbitals of the N substituting for O couple with the O $2p$ orbitals and lead to N-related bands above the original valence band, resulting in photoabsorption in the upper part of the visible spectrum. Similar effects have also been proposed to occur for C and S additions [15, 16]. Transition-metal and noble-metal additions, such as Cr, Co, V, Fe, Au, Ag, Cu, Pt and Pd [7, 17–20], have also

been proposed to bring the optical absorption in TiO_2 into the visible region. In the cases that have been tried in the laboratory [10–13, 17, 20], the reported enhancements in the visible-light absorption are not substantial, and limited to wavelengths longer than 450 nm (i.e., photon energies higher than 2.75 eV). Such slight improvements were attributed in part to the low solubility and insufficient redshift of the band gap in the case of N [10–13], or to introducing localized in-gap states close to the conduction band and incorporating on the surface and blocking the catalytic sites in the case of transition metals [17, 20]; visible-light responsiveness of TiO_2 with noble-metal additions was attributed to noble-metal related surface plasmons [20] instead of absorption in the TiO_2 .

More recently, addition of post transition metals to TiO_2 , such as Bi, has also been considered, aiming at enhancing visible-light absorption and improving its photocatalytic efficiency [21–25]. Earlier work on the effects of adding Bi to TiO_2 reported an increase of a factor of 10 in the hydrogen photo-generation rate and a remarkable photocurrent enhancement, with optimum results obtained for 1% mol Bi content [21]. However, it remains unclear if these improvements came from Bi at the surface or Bi incorporated in the bulk. Subsequent experiments of Bi-added TiO_2 thin films and nanoparticles also reported improvements in photocatalytic efficiency, yet the proposed mechanisms either involved the assumption of a Bi-related band near the TiO_2 conduction band [22, 23] or Bi-metal/ Bi_2O_3 formation at the surface [25]. The microscopic mechanism, local structure, and effects of Bi on the electronic structure of TiO_2 are yet to be resolved.

Inspired by these earlier promising results, we per-

formed density functional theory (DFT) and hybrid functional calculations to study the structural, electronic, and optical properties of dilute $\text{Ti}_{1-x}\text{Bi}_x\text{O}_2$ alloys, in rutile and anatase phases. For comparison, we also performed calculations for dilute $\text{TiO}_{2-y}\text{N}_y$ alloys, focusing on the formation enthalpy of these two systems as function of Bi and N concentrations, and their electronic and optical properties. We find that Bi introduces a partially occupied intermediate valence band, detached from the original O $2p$ valence band, lying almost in the middle of the band gap, leaving the conduction band unchanged. This intermediate valence band leads to high absorption coefficients in the visible range, making $\text{Ti}_{1-x}\text{Bi}_x\text{O}_2$ much more robust for visible-light water splitting than $\text{TiO}_{2-y}\text{N}_y$ alloys.

COMPUTATIONAL APPROACH

The calculations are based on density functional theory [26, 27] within the Perdew, Burke, and Ernzerhof exchange and correlation functional revised for solids (PBEsol) [28] and the hybrid functional of Heyd, Scuseria, and Ernzerhof (HSE06) [29, 30], implemented with projected augmented wave (PAW) potentials [31] in the VASP code [32, 33]. The stress tensor and the atomic forces were relaxed using PBEsol with a cutoff energy of 620 eV for the plane-wave basis set. We employed a \mathbf{k} -point mesh of $5 \times 5 \times 9$ for integrations over the Brillouin zone of the 6-atom primitive cell of rutile TiO_2 , and maintain the same \mathbf{k} -mesh density for anatase and the supercells containing Bi or N.

Since PBEsol severely underestimates band gaps, we employ the HSE06 hybrid functional to describe the electronic properties of rutile and anatase TiO_2 , $\text{Ti}_{1-x}\text{Bi}_x\text{O}_2$ and $\text{TiO}_{2-y}\text{N}_y$. Under this approximation, the exchange potential is divided in short and long-range parts by a screening parameter $\omega = 0.206 \text{ \AA}^{-1}$ [29, 30]. In the short-range part, non-local Hartree-Fock exchange is mixed with semi-local PBE exchange [34] in a ratio of 25%/75%; the long-range part is described by the PBE functional. For the electronic structure calculations, with the HSE06 hybrid functional, the cutoff energy was reduced to 470 eV. The density of states (DOS) for the primitive cells and the supercells representing the alloys were calculated using Γ -centered \mathbf{k} -point meshes that are equivalent to a $11 \times 11 \times 17$ mesh for the rutile TiO_2 6-atom primitive cell.

The dilute alloys in the rutile and anatase phases, $r\text{-Ti}_{1-x}\text{Bi}_x\text{O}_2$, $a\text{-Ti}_{1-x}\text{Bi}_x\text{O}_2$, $r\text{-TiO}_{2-y}\text{N}_y$, and $a\text{-TiO}_{2-y}\text{N}_y$, were simulated using special quasi-random structures [35, 36] to represent random arrangements of Bi or N. For the rutile phase we use a supercell of 192 atoms where we replaced 1, 2, and 3 Ti with Bi atoms to simulate concentrations of 1.6%, 3.1%, and 4.7%; equivalently we replaced 2, 4, and 6 O with N atoms. For the anatase

phase, we used a supercell of 108 atoms where we replaced 1 and 2 Ti with Bi atoms to simulate concentrations of 2.8% and 5.6%; equivalently we replaced 2 and 4 O with N atoms.

Since Bi and N are aliovalent species in TiO_2 , the calculations for the density of states and optical properties of $\text{Ti}_{1-x}\text{Bi}_x\text{O}_2$ and $\text{TiO}_{2-y}\text{N}_y$ alloys were performed for charge compensated closed shell systems, i.e., with the intermediate valence bands completely filled, assuming that, in practice, donor defects such as oxygen vacancies will be present as compensation centers. This avoids the difficulties of having to calculate dielectric matrices for metallic systems. The optical properties were computed with the tetrahedral smearing method, phonon assisted transitions and exciton effects were neglected, as these effects will not affect our conclusions.

Finally, due to the high computation cost to calculate the dielectric matrix with required high-density \mathbf{k} -point mesh for the alloy supercells using HSE06, we performed the calculations with PBEsol and used a scissors operator to the PBEsol results and shifted the optical absorption coefficient based on the difference between the band gap obtained in HSE06 and PBEsol. This approach is expected to not affect the intensity of the absorption coefficient near the band gap or elsewhere.

RESULTS AND DISCUSSION

Structural properties of $\text{Ti}_{1-x}\text{Bi}_x\text{O}_2$ and $\text{TiO}_{2-y}\text{N}_y$ alloys and their formability

The most common phase of bulk TiO_2 is rutile ($r\text{-TiO}_2$), whereas anatase ($a\text{-TiO}_2$) is mostly found in thin-film and nanostructure forms. $r\text{-TiO}_2$ belongs to $P4_2/mnm$ space group and contains 6 atoms in the primitive cell, while $a\text{-TiO}_2$ belongs to $I4_1/amd$ space group and contains 12 atoms in the primitive cell. In both phases, each Ti atom is surrounded by six O atoms forming edge-sharing octahedra, which are almost perfect in rutile and highly distorted in anatase. Each O atom is bonded to three Ti atoms in planar configurations. Based on atomic radii [37], Bi (1.6 Å) is expected to incorporate on the Ti (1.4 Å) sites, while N (0.65 Å) is expected to substitute for O (0.60 Å).

The calculated lattice parameters for $r\text{-TiO}_2$ and $a\text{-TiO}_2$, listed in Table I, are in good agreement with the experimental data [38, 39]. Adding Bi to TiO_2 , with each Bi substituting on a Ti site, leads to a sizable increase in lattice parameters, attributed to the large atomic radius of Bi compared to that of Ti. In contrast, adding N, replacing O, leads to only slight increase in lattice parameters and in the volume per formula unit. For example, for N concentration of $y = 5.6\%$ in $a\text{-TiO}_{2-y}\text{N}_y$, we find a volume expansion of only 0.20%, while for Bi concentration of $x = 5.6\%$ in $a\text{-Ti}_{1-x}\text{Bi}_x\text{O}_2$, the volume

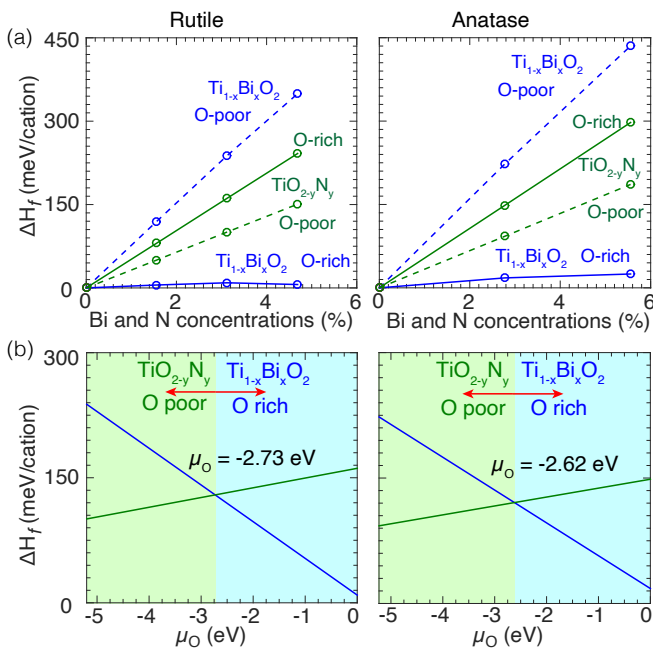


FIG. 1. Formation enthalpy (ΔH_f) of $\text{Ti}_{1-x}\text{Bi}_x\text{O}_2$ and $\text{TiO}_{2-y}\text{N}_y$ alloys. (a) Formation enthalpy as function of Bi and N content for the alloys in rutile (r -) and anatase (a -) phases. The continuous lines refer to O-rich limit condition, while the dashed lines refer to the O-poor limit condition. (b) Formation enthalpy as function of chemical potential μ_{O} for Bi and N concentrations of 3.13% for r - $\text{Ti}_{1-x}\text{Bi}_x\text{O}_2$ and r - $\text{TiO}_{2-y}\text{N}_y$, and 2.8% for the alloys in the anatase phase. The crossing point in μ_{O} indicates the chemical potential value above which $\text{Ti}_{1-x}\text{Bi}_x\text{O}_2$ alloys have lower formation enthalpy than $\text{TiO}_{2-y}\text{N}_y$, showing that the former are more favorable to form in more oxidizing conditions.

TABLE I. Lattice parameters a_0 and c_0 and volume of r - TiO_2 (rutile), a - TiO_2 (anatase) and $\text{Ti}_{1-x}\text{Bi}_x\text{O}_2$ and $\text{TiO}_{2-y}\text{N}_y$ alloys for different Bi and N concentrations (x or y). The experimental data for r - TiO_2 and a - TiO_2 from Refs. [38, 39] are also listed.

Material	x or y (%)	a_0 (Å)	c_0 (Å)	Volume (Å ³ /f.u.)
r - TiO_2		4.584	2.937	30.86
r - TiO_2 (exp.)		4.594	2.959	31.22
r - $\text{Ti}_{1-x}\text{Bi}_x\text{O}_2$	1.6	4.593	2.945	31.06
r - $\text{Ti}_{1-x}\text{Bi}_x\text{O}_2$	3.1	4.604	2.952	31.28
r - $\text{Ti}_{1-x}\text{Bi}_x\text{O}_2$	4.7	4.617	2.960	31.55
r - $\text{TiO}_{2-y}\text{N}_y$	1.6	4.584	2.939	30.87
r - $\text{TiO}_{2-y}\text{N}_y$	3.1	4.585	2.939	30.90
r - $\text{TiO}_{2-y}\text{N}_y$	4.7	4.587	2.940	30.93
a - TiO_2		3.765	9.538	33.81
a - TiO_2 (exp.)		3.784	9.515	34.06
a - $\text{Ti}_{1-x}\text{Bi}_x\text{O}_2$	2.8	3.782	9.579	34.25
a - $\text{Ti}_{1-x}\text{Bi}_x\text{O}_2$	5.6	3.800	9.624	36.73
a - $\text{TiO}_{2-y}\text{N}_y$	2.8	3.767	9.543	33.86
a - $\text{TiO}_{2-y}\text{N}_y$	5.6	3.768	9.545	33.88

increases by 8.6%.

Neglecting the charge state of the Bi addition, the for-

mation enthalpy of the dilute $\text{Ti}_{1-x}\text{Bi}_x\text{O}_2$ alloys are calculated using:

$$\begin{aligned} \Delta H_f(\text{Ti}_{1-x}\text{Bi}_x\text{O}_2) = & E_{tot}(\text{Ti}_{1-x}\text{Bi}_x\text{O}_2) - E_{tot}(\text{TiO}_2) \\ & + n[E_{tot}(\text{Ti}) - E_{tot}(\text{Bi})] \\ & + n(\mu_{\text{Ti}} - \mu_{\text{Bi}}), \end{aligned} \quad (1)$$

where $E_{tot}(\text{Ti}_{1-x}\text{Bi}_x\text{O}_2)$ is the total energy of the supercell representing the alloy, $E_{tot}(\text{TiO}_2)$ is the total energy of pristine TiO_2 using the same supercell size. The chemical potentials μ_{Ti} and μ_{Bi} are referenced to the total energies of Ti and Bi bulk metallic phases ($E_{tot}(\text{Ti})$ and $E_{tot}(\text{Bi})$), with $\mu_{\text{Ti}} \leq 0$ and $\mu_{\text{Bi}} \leq 0$. Similar expression is used to calculate the formation enthalpy of the dilute $\text{TiO}_{2-y}\text{N}_y$ alloys. The variation of the chemical potentials μ_{Ti} , μ_{O} , μ_{Bi} , and μ_{N} are restricted by the stability of TiO_2 and the formation of the secondary phases Bi_2O_3 and TiN . For example, in the O-rich limit condition we have: $\mu_{\text{O}} = 0$, $\mu_{\text{Ti}} = \Delta H_f(\text{TiO}_2)$, $\mu_{\text{Bi}} = \frac{1}{2}\Delta H_f(\text{Bi}_2\text{O}_3)$, and $\mu_{\text{N}} = 0$; in the O-poor limit we have: $\mu_{\text{O}} = \frac{1}{2}\Delta H_f(\text{TiO}_2)$, $\mu_{\text{Ti}} = 0$, $\mu_{\text{Bi}} = 0$, and $\mu_{\text{N}} = \Delta H_f(\text{TiN})$. $\Delta H_f(\text{TiO}_2)$, $\Delta H_f(\text{Bi}_2\text{O}_3)$, and $\Delta H_f(\text{TiN})$ are the formation enthalpy of TiO_2 , Bi_2O_3 , and TiN , respectively. The results for alloy formation enthalpy (ΔH_f) as function of concentration of Bi and N in the O-rich and O-poor limit conditions are shown in Fig. 1(a).

The chemical potential μ_{O} plays important role in the incorporation of Bi and N in TiO_2 . Since Bi occupies the Ti site, its incorporation is most favorable in O-rich (Ti-poor) conditions, while the incorporation of N is most favorable in O-poor (Ti-rich) conditions since it sits on the O site. As seen in Fig. 1(a), we find that the formation enthalpy of the dilute $\text{Ti}_{1-x}\text{Bi}_x\text{O}_2$ alloys varies over a wider range from O-rich to O-poor limit conditions compared to the $\text{TiO}_{2-y}\text{N}_y$ alloys. A crossing in the formation enthalpy plot as function of μ_{O} is thus expected. This crossing indicates the μ_{O} value above which the formation enthalpy of the $\text{Ti}_{1-x}\text{Bi}_x\text{O}_2$ alloy is lower than that of the $\text{TiO}_{2-y}\text{N}_y$ for the same Bi and N concentration. Since the formation enthalpy varies linearly with concentration in the dilute regime considered here, the μ_{O} value at the crossing does not depend on the Bi and N content, but it is different for the two phases. We find that $\mu_{\text{O}} = -2.73$ eV for rutile and -2.62 eV for anatase. Considering typical growth conditions of TiO_2 thin films by molecular beam epitaxy [12, 13], for example, with temperature in the range of 400–700°C and pressure of 10^{-3} – 10^{-7} torr, μ_{O} for O_2 gas falls in the range of -1.7 eV to -0.9 eV, being closer to the O-rich limit, and favoring Bi incorporation. The results in Fig. 1(a) also show that it cost less energy to incorporate Bi on the octahedral chemical environment of rutile than on the distorted octahedral environment of the anatase phase. In contrast, the formation enthalpy for the incorporation of N in r - TiO_2 and a - TiO_2 are almost the same for a given value of μ_{O} , which

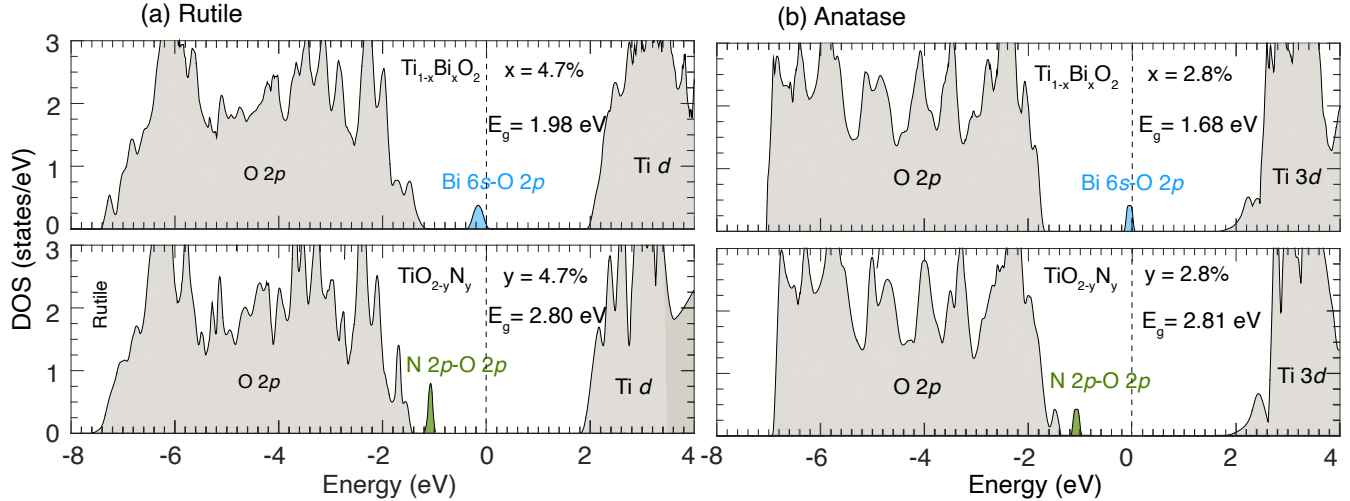


FIG. 2. Electronic density of states (DOS) for dilute $\text{Ti}_{1-x}\text{Bi}_x\text{O}_2$ and $\text{TiO}_{2-y}\text{N}_y$ alloys in (a) rutile and (b) anatase phases. The zero in energy axes is set to the top of the intermediate valence band in the $\text{Ti}_{1-x}\text{Bi}_x\text{O}_2$ alloys. The DOS of $\text{Ti}_{1-x}\text{Bi}_x\text{O}_2$ and $\text{TiO}_{2-y}\text{N}_y$ in the same phase were aligned using the low lying O $2s$ bands located around -19 eV. The results show that $\text{Ti}_{1-x}\text{Bi}_x\text{O}_2$ alloys show smaller energy differences between the intermediate valence band and the conduction band than $\text{TiO}_{2-y}\text{N}_y$ alloys. In these calculations electrons were added to have fully occupied intermediate valence bands with Bi and N, representing electronic compensated dilute alloys without explicitly adding the compensating centers, such as oxygen vacancies[40] for example.

we attribute to the similarity between the anion chemical environment in rutile and anatase.

Both $\text{Ti}_{1-x}\text{Bi}_x\text{O}_2$ and $\text{TiO}_{2-y}\text{N}_y$ alloys have been demonstrated [10–13, 22–25], with Bi and N concentrations of up to a few atomic percent. For Bi, it was found a maximum solubility around 5% before formation of a secondary phase occurs[24]. These dilute concentrations are consistent with the values of formation enthalpy shown in Fig. 1. Our results show a large variation of the formation enthalpy of $\text{Ti}_{1-x}\text{Bi}_x\text{O}_2$ with μ_{O} , and indicate that for maximizing the Bi concentration, O-rich growth or deposition conditions should be employed.

Electronic structure and optical properties of $\text{Ti}_{1-x}\text{Bi}_x\text{O}_2$ and $\text{TiO}_{2-y}\text{N}_y$ alloys

For the effects of adding Bi on the electronic and optical properties of TiO_2 , our results show that Bi leads to remarkably larger redshift in band gap and optical absorption than N. The calculated density of states (DOS) of dilute $\text{Ti}_{1-x}\text{Bi}_x\text{O}_2$ and $\text{TiO}_{2-y}\text{N}_y$ with $x = y = 4.7\%$ for rutile and $x = y = 2.8\%$ for anatase are shown in Fig 2.

In TiO_2 , the band gap of ~ 3 eV separates the occupied valence band, derived mostly from O $2p$ orbitals, from the unoccupied conduction band derived mostly from the Ti $3d$ orbitals. For r - TiO_2 , the calculated band gap is 3.10 eV, and 3.35 eV for a - TiO_2 , compared to the experimental values of 3.02 eV [8] and 3.20 eV, respectively. When Bi is incorporated into TiO_2 , forming a dilute $\text{Ti}_{1-x}\text{Bi}_x\text{O}_2$ alloy, a partially occupied intermediate band is created

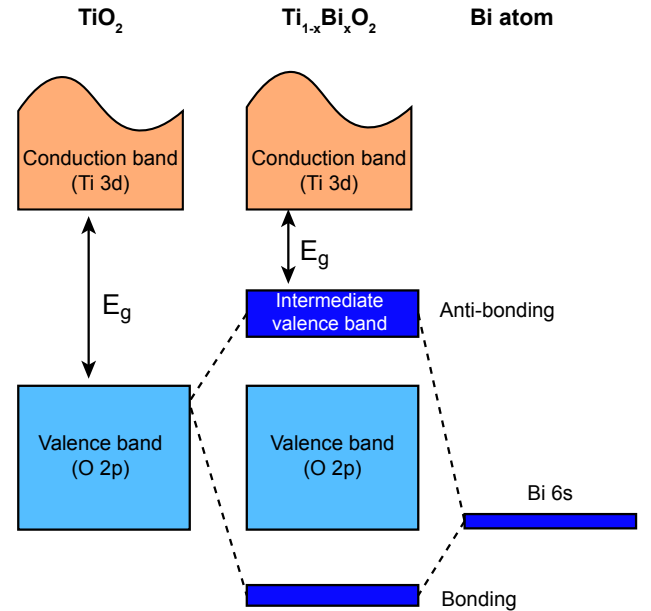


FIG. 3. Schematic representation of the coupling between the Bi $6s$ and O $2p$ forming the intermediate valence band in dilute $\text{Ti}_{1-x}\text{Bi}_x\text{O}_2$ alloys, considerably reducing the excitation energy to the conduction band, yet leaving the position of the conduction band unchanged.

and located in the band gap, closer to the valence band. This intermediate band is derived from the coupling between the O $2p$ and the low lying Bi $6s$ bands—the later

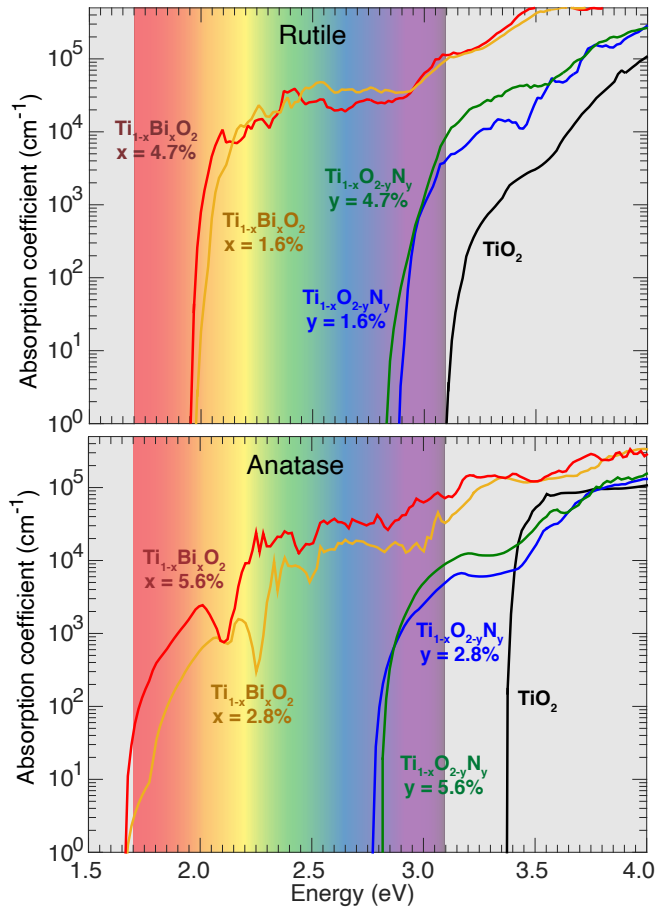


FIG. 4. Calculated absorption coefficient (averaged over the three cartesian directions) as a function of photon energy for TiO_2 , $\text{Ti}_{1-x}\text{Bi}_x\text{O}_2$ and $\text{TiO}_{2-y}\text{N}_y$ with Bi and N concentrations of 1.6 and 4.7% in rutile and 2.8 and 5.6% in anatase crystal structure. The colored region indicate the visible-light spectrum.

is located between -9 and -10 eV below the top of the valence band, as schematically shown in Fig. 3. The partially occupied intermediate valence band in $\text{TiO}_{2-y}\text{N}_y$ alloys, for comparison, is much closer to the valence band, visibly modifying the top of the O $2p$ band, where a small shoulder in the DOS can be distinguished.

The intermediate valence band significantly reduces the excitation energy to the conduction band as indicated in Fig. 2 and Fig. 3, and this effect is remarkably stronger in $\text{Ti}_{1-x}\text{Bi}_x\text{O}_2$ than in $\text{TiO}_{2-y}\text{N}_y$. Note that the distance between the O $2p$ and the Ti $3d$ bands remains almost unchanged, indicating that adding Bi or N only affects the highest occupied bands and does not change the position of the conduction band with respect to the vacuum level. This is a desirable effect in photoelectrochemical devices based on TiO_2 , enabling visible-light absorption while keeping the conditions that favor the redox potentials for water splitting [6].

Our results also show that adding Bi not only enables

visible-light absorption over a wider range in the spectrum, but also leads to a significantly increase in the absorption coefficient near the effective band gap (between the intermediate valence band and the conduction band), compared to adding N. The calculated absorption coefficients for $\text{Ti}_{1-x}\text{Bi}_x\text{O}_2$, $\text{TiO}_{2-y}\text{N}_y$, and TiO_2 for comparison, are shown in Fig. 4. Having the system electronically compensated facilitates these calculations, and the results were averaged over the three orthogonal directions, which can be argued to better represent the absorption in polycrystalline films or nanostructures.

For bulk TiO_2 , the optical band gap does not coincide with the fundamental band gap, as observed for several other oxides, including SnO_2 , In_2O_3 , PbO_2 [41–44]. For $r\text{-TiO}_2$, the dipole transition from valence-band maximum to conduction-band minimum at Γ is forbidden due to symmetry considerations; however, transitions in the vicinity of the Γ point are allowed (yet with amplitude smaller than $\sim 10^{-4} \text{ cm}^{-1}$) and, due to the relatively small dispersion of the valence and conduction bands, the onset in the optical absorption coefficient is slightly shifted, by ~ 0.1 eV, to higher energies with respect to the fundamental band gap, as shown in Fig. 4(a). For $a\text{-TiO}_2$, the dipole matrix element for the minimum-energy transition from valence to conduction band is also forbidden by symmetry, and due to larger dispersion of the valence and conduction bands, the optical gap is shifted to higher energies by ~ 0.4 eV with respect to the fundamental band gap, as shown in Fig. 4(b). These results corroborate the fact that TiO_2 by itself is so inefficient for visible-light photoelectrochemical processes.

For dilute $\text{TiO}_{2-y}\text{N}_y$ alloys, the N-related intermediate valence band leads to a reduction in the effective band gap, indicating that the alloy absorbs visible light, yet restricted to photons of relatively high energies. As shown in Fig. 4, $r\text{-TiO}_{2-y}\text{N}_y$ alloys start absorbing visible light at ~ 2.7 eV (459 nm), while $a\text{-TiO}_{2-y}\text{N}_y$ alloys start at ~ 2.6 eV (477 nm). The position of the onset of optical absorption varies only slightly with N concentration; nevertheless, the amplitude of the absorption coefficients increases with N content as seen in Fig. 4. Experimentally, it is known that adding N to $a\text{-TiO}_2$ leads to visible light absorption starting at around 2.5 eV [10, 11]. This is in good agreement with our calculations considering that the calculated band gap of $a\text{-TiO}_2$ using HSE06 is 0.15 eV higher than the experimental value.

In the case of dilute $\text{Ti}_{1-x}\text{Bi}_x\text{O}_2$ alloys, the redshift in the absorption coefficient is significantly larger than in $\text{TiO}_{2-y}\text{N}_y$. The Bi-related intermediate valence band lies almost in the middle of TiO_2 band gap, and the predicted onset of optical absorption occurs at 2.0 eV (620 nm) in $r\text{-Ti}_{1-x}\text{Bi}_x\text{O}_2$ and 1.7 eV (719 nm) in $a\text{-Ti}_{1-x}\text{Bi}_x\text{O}_2$. It the later, it covers almost all the visible spectrum. Similar to the N case, the position of the onset of optical absorption does not change with Bi content in the dilute regime considered here, yet high amplitudes in the ab-

sorption coefficient near the threshold are obtained with higher Bi concentrations. Our results explain experimental observations of Bi-doped TiO₂ indicating a band gap of 2.05 eV (600 nm) [23], yet the microscopic mechanism has not been addressed.

The combination of high optical absorption in the visible for both rutile and anatase phases of dilute Ti_{1-x}Bi_xO₂ alloys, and the fact that adding Bi does not affect the position of the conduction band make these alloys promising candidates for photocatalysis and water splitting. The comparison with TiO_{2-y}N_y clearly shows the superiority of adding Bi instead of N, leading to significantly higher absorption and wider range in the visible, almost reaching the IR region of the spectrum [Fig. 4(b)].

CONCLUSIONS

In summary, using DFT and hybrid functional calculations we show that adding Bi leads to significantly more efficient visible-light absorption than adding N to TiO₂. Our results for *a*-Ti_{1-x}Bi_xO₂ alloy with 5.6% shown onset of optical absorption at ~ 1.7 eV, which is near the upper limit of the IR spectrum, thus efficiently covering almost the whole visible region. As with N, adding Bi does not affect the position of the conduction band, offering an optimum straddling of the redox potentials for water splitting. The incorporation of Bi is predicted to be most favorable in oxidizing conditions in contrast to N incorporation. Our results not only explain the available experimental data on Bi-doped TiO₂, but also provide the microscopic mechanisms for the observed enhancement of visible-light absorption, calling for further experimental efforts to study the stability and performance of Bi-added TiO₂ in photocatalysis and water splitting.

ACKNOWLEDGMENTS

This work was supported by the NSF Early Career Award grant no. DMR-1652994, the Extreme Science and Engineering Discovery Environment (XSEDE) supported by National Science Foundation grant number ACI-1053575, and the Information Technologies (IT) resources at the University of Delaware. FPS acknowledges support from FAPESP grant no. 2019/21656-8.

[1] W. A. Braff, J. M. Mueller, and J. E. Trancik, *Nat. Clim. Chang.* **6**, 964 (2016).
 [2] S. Ye, C. Ding, R. Chen, F. Fan, P. Fu, H. Yin, X. Wang, Z. Wang, P. Du, and C. Li, *J. Am. Chem. Soc.* **140**, 3250 (2018).

[3] T. Jafari, E. Moharreri, A. S. Amin, R. Miao, W. Song, and S. L. Suib, *Molecules* **21** (2016).
 [4] A. Fujishima and K. Honda, *Nature* **238**, 37 (1972).
 [5] M. Ni, M. K. Leung, D. Y. Leung, and K. Sumathy, *Renew. Sust. Energ. Rev.* **11**, 401 (2007).
 [6] C. Jiang, S. J. Moniz, A. Wang, T. Zhang, and J. Tang, *Chem. Soc. Rev.* **46**, 4645 (2017).
 [7] C. Cheng, W.-H. Fang, R. Long, and O. V. Prezhdo, *JACS Au* **1**, 550 (2021).
 [8] J. Pascual, J. Camassel, and H. Mathieu, *Phys. Rev. B* **18**, 5606 (1978).
 [9] H. Tang, H. Berger, P. Schmid, F. Lévy, and G. Burri, *Solid State Commun.* **87**, 847 (1993).
 [10] S. Sato, *Chem. Phys. Lett.* **123**, 126 (1986).
 [11] R. Asahi, T. Morikawa, T. Ohwaki, K. Aoki, and Y. Taga, *Science* **293**, 269 (2001).
 [12] S. Chambers, S. Cheung, V. Shutthanandan, S. Thevuthasan, M. Bowman, and A. Joly, *Chem. Phys.* **339**, 27 (2007).
 [13] S. Cheung, P. Nachimuthu, A. Joly, M. Engelhard, M. Bowman, and S. Chambers, *Surf. Sci.* **601**, 1754 (2007).
 [14] J. B. Varley, A. Janotti, and C. G. Van de Walle, *Adv. Mater.* **23**, 2343 (2011).
 [15] S. Piskunov, O. Lisovski, J. Begens, D. Bocharov, Y. F. Zhukovskii, M. Wessel, and E. Spohr, *J. Phys. Chem. C* **119**, 18686 (2015).
 [16] N. Umezawa, A. Janotti, P. Rinke, T. Chikyow, and C. G. Van de Walle, *Appl. Phys. Lett.* **92**, 041104 (2008).
 [17] X. Z. Li and F. B. Li, *Environ. Sci. Technol.* **35**, 2381 (2001).
 [18] A. Fuerte, M. D. Hernández-Alonso, A. J. Maira, A. Martínez-Arias, M. Fernández-García, J. C. Conesa, and J. Soria, *Chem. Commun.*, 2718 (2001).
 [19] D. Dvoranová, V. Brezová, M. Mazúr, and M. A. Malati, *Appl. Catal., B* **37**, 91 (2002).
 [20] M. Pelaez, N. T. Nolan, S. C. Pillai, M. K. Seery, P. Falaras, A. G. Kontos, P. S. Dunlop, J. W. Hamilton, J. Byrne, K. O'Shea, M. H. Entezari, and D. D. Dionysiou, *Appl. Catal., B* **125**, 331 (2012).
 [21] Y. Wu, G. Lu, and S. Li, *J. Phys. Chem. C* **113**, 9950 (2009).
 [22] S. Sajjad, S. A. K. Leghari, F. Chen, and J. Zhang, *Chem. Eur. J.* **16**, 13795 (2010).
 [23] Q. M. Kang, B. L. Yuan, J. G. Xu, and M.-L. Fu, *Catal. Lett.* **141**, 1371 (2011).
 [24] M.-C. Wu, Y.-H. Chang, and T.-H. Lin, *Jpn. J. Appl. Phys.* **56**, 04CJ01 (2017).
 [25] D. Xu, Y. Hai, X. Zhang, S. Zhang, and R. He, *Appl. Surf. Sci.* **400**, 530 (2017).
 [26] P. Hohenberg and W. Kohn, *Phys. Rev.* **136**, B864 (1964).
 [27] W. Kohn and L. J. Sham, *Phys. Rev.* **140**, A1133 (1965).
 [28] J. P. Perdew, A. Ruzsinszky, G. I. Csonka, O. A. Vydrov, G. E. Scuseria, L. A. Constantin, X. L. Zhou, and K. Burke, *Phys. Rev. Lett.* **100**, 136406 (2008).
 [29] J. Heyd and G. E. Scuseria, *J. Chem. Phys.* **120**, 7274 (2004).
 [30] J. Heyd, G. E. Scuseria, and M. Ernzerhof, *J. Chem. Phys.* **124**, 219906 (2006).
 [31] P. E. Blöchl, *Phys. Rev. B* **50**, 17953 (1994).
 [32] G. Kresse and J. Hafner, *Phys. Rev. B* **48**, 13115 (1993).
 [33] G. Kresse and J. Furthmüller, *Phys. Rev. B* **54**, 11169 (1996).

- [34] J. P. Perdew, K. Burke, and M. Ernzerhof, *Phys. Rev. Lett.* **77**, 3865 (1996).
- [35] A. Zunger, S.-H. Wei, L. G. Ferreira, and J. E. Bernard, *Phys. Rev. Lett.* **65**, 353 (1990).
- [36] A. van de Walle, P. Tiwary, M. de Jong, D. Olmsted, M. Asta, A. Dick, D. Shin, Y. Wang, L.-Q. Chen, and Z.-K. Liu, *Calphad* **42**, 13 (2013).
- [37] J. C. Slater, *J. Chem. Phys.* **41**, 3199 (1964).
- [38] R. Wyckoff, *Crystal structures*, Vol. 2 (Wiley, New York, 1963).
- [39] M. Horn, C. Schwerdtfeger, and E. Meagher, *Z. Kristallogr.* **136**, 273 (1972).
- [40] A. Janotti, J. B. Varley, P. Rinke, N. Umezawa, G. Kresse, and C. G. Van de Walle, *Phys. Rev. B* **81**, 085212 (2010).
- [41] A. Walsh, J. L. F. Da Silva, S. H. Wei, C. Körber, A. Klein, L. F. J. Piper, A. Demasi, K. E. Smith, G. Panaccione, P. Torelli, D. J. Payne, A. Bourlange, and R. G. Egdell, *Phys. Rev. Lett.* **100**, 167402 (2008).
- [42] D. O. Scanlon, A. B. Kehoe, G. W. Watson, M. O. Jones, W. I. F. David, D. J. Payne, R. G. Egdell, P. P. Edwards, and A. Walsh, *Phys. Rev. Lett.* **107**, 246402 (2011).
- [43] F. P. Sabino, R. Besse, L. N. Oliveira, S.-H. Wei, and J. L. F. Da Silva, *Phys. Rev. B* **92**, 205308 (2015).
- [44] F. P. Sabino, L. N. Oliveira, S.-H. Wei, and J. L. F. Da Silva, *J. Phys.: Condens. Matter* **29**, 085501 (2017).